Turkish Journal of Chemistry

http://journals.tubitak.gov.tr/chem/

Research Article

Turk J Chem
(2021) 45: 683-693

doi:10.3906/kim-2101-30

The impact of alkaline earth oxides on Bi_2O_3 and their catalytic activities in photodegradation of Bisphenol A

Ümran ÜNLÜ, Sevgi KEMEÇ, Gülin Selda POZAN SOYLU*
Chemical Engineering Department Engineering Faculty, İstanbul University, Cerrahpaşa, İstanbul, Turkey

Received: 12.01.2021 • **Accepted/Published Online:** 17.02.2021 • **Final Version:** 30.06.2021

Abstract: The BPA into wastewater has posed a threat to environment and human health. Hence, we aimed to eliminate BPA in a short time and with a rapid degradation rate from food wastewater. Herein, the effects of different alkaline-earth oxide doped with Bi_2O_3 nanoparticles on the photocatalytic degradation of bisphenol A were investigated. SrO-Bi_2O_3, CaO-Bi_2O_3, and MgO-Bi_2O_3 binary oxides were prepared by wet-impregnation method. The structural and optical features of catalysts were clarified BET, XRD, DRS, FT-IR, PL, and SEM techniques. The photocatalytic activities of catalysts were compared for different light sources. Considering that the characterization analysis and experimental results, the highly improved photocatalytic activity was mainly attributed to the effective structure of the SrO-Bi_2O_3 binary oxide and the strong alkali properties in the nanocomposite. Obviously, 5wt% SrO-Bi_2O_3 photocatalyst showed more excellent degradation performance and highest degradation reaction rate (0.21 mg l^{-1} min^{-1}) within 30 min. It was observed that the photocatalytic activity improved by the additive of alkaline oxide on Bi_2O_3.

Key words: Photocatalysis; alkaline earth oxide; Bisphenol A; degradation; UV-B irradiation

1. Introduction

Bisphenol-A or BPA which can be synthesized organic compound, has the formula $(CH_3)_2C(C_6H_4OH)_2$. Research shows that BPA is one of the chemicals with the highest production capacity than other chemicals throughout the world [1,2]. As mentioned in the world health organization, BPA is a chemical utilized chiefly as a monomer in the production of polymers such as epoxy resins and polycarbonate plastic (PC). Additionally, it has uses in polysulfone, polyacrylate resins, polyester, and flame retardants. Polycarbonate (PC) is thoroughly used in food contact materials like baby bottles, tableware, food containers, drink bottles, processing materials, and water pipes. Epoxy resins are utilized as preservative linings for a diversity of canned foods and drinks and as a coating on lids of glass jars and bottles (WHO, INFOSAN 2009)[1] [2]. According to the researchers BPA can mimic the actions of estrogen, binding to the same receptor in the body. So, degradation of BPA is important status [3]. Bisphenol-A is known to be one of the notable EDC (endocrine disrupting compounds) and harmful to human health, agriculture, and environment. BPA has stable structure so, degradation of Bisphenol A is difficult [4–6]. Compounds such as BPA at low concentrations have been found to be highly toxic, poorly biodegradable, and present carcinogenic properties.

Pollutants like BPA effecting the environment are serious problem in improving countries. Furthermore, the rising population and increasing requisitions for water resources cause that there is a constantly growing in this problem. BPA is a substance that affects human health and there is a problem such as global warming in our world, so the treatment of wastewater has become very important. Development of environmentally friendly methods for removal of BPA is one of the most relevant issues in the field of reaching the clean water. Therefore, various methods like chemical oxidation [6–8], physical elimination development [9], biodegradation [10], adsorption [11], and photodegradation have been developed for the degradation of BPA [12].

[1] World Health Organization and Food and Agriculture Organization of the United Nations. BISPHENOL A (BPA) - Current state of knowledge and future actions. International Food Safety Authorities Network 2009; Information Note No. 5/2009 - Bisphenol A. [Online] https://www.who.int/food-safety/publications/fs_management/No_05_Bisphenol_A_Nov09_en.pdf. [accessed on _____].

* Correspondence: gpozan@istanbul.edu.tr

Previous studies have shown that photodegradation gives good results. So, heterogeneous photocatalytic oxidation has been seen as potential effective technique to deteriorate environmental pollutant. With this in mind, we prefer heterogeneous photocatalytic degradation which is more advantageous than the other methods since it is low cost, reusable, provides complete degradation, and it is eco-friendly method.

BPA can be co-existing with other contaminants, so more selective catalysts should be used. During the study we used alkali metal oxides on bismuth oxide. The alkaline earth metals used in this study are often white in color, soft, and workable. In addition to being less reactive (prone to reactions) than alkali metals, their melting and boiling temperatures are also lower. Ionization energies are also higher than alkali metals. SrO impregnated with different proportions on Bi_2O_3 showed great selectivity and was successful in a short time. In addition to these different catalysts were used as the main catalyst [13–15]. When the previous studies were examined, titanium oxide was used many times as the main catalyst, as it has an extended band gap [14–17]. In particular, Bi_2O_3 has been used since it is a nontoxic and noncarcinogenic compound and has high photocatalytic activity with a bandwidth ranging from 2.0–2.8 eV [18–21].

The use of binary metal oxides as photocatalysts has been made widely for decades because of the fact that the morphological properties of the individual oxides can be changed due to the formation of new sites in the interface between the components, or by the incorporation of one oxide into the lattice of the other. They also found that this enhancement was attributed to gradually increasing shift of the conduction bands with increasing metal oxide contents, so resulting in a stronger reduction power of photogenerated electrons and promoting the improved photocatalytic activity.

In the current study, MxOy–Bi_2O_3 (M: Ca, Mg, Sr) photocatalysts with various loading of the metal oxides were prepared by impregnation method. The catalytic activities of synthesized materials were investigated by using UV irradiation. The complete degradation of pollutants such as BPA by photocatalytic methods is a promising solution for environmental problems and human health. In this study, the purpose is to explain the impact of parameters such as the use of different types of metal oxides and the percentage of metal oxides on the photooxidation of BPA. Another aim is to reduce the concentration of BPA. This is due to the fact that BPA has pollutants for the environment and harmful effects on human health. Moreover, the relationships between the catalyst morphologies and the photocatalytic activities were also investigated by using varied characterization methods such as scanning electron microscope (SEM), diffuse reflectance spectroscopy (DRS), Brunauer, fourier transform infrared (FTIR), Emmet and Teller (BET), and X-Ray diffraction (XRD).

2. Experimental and methods

2.1. Materials

In this experimental study, essential materials were supplied commercially and utilized without additional purification process. These materials are bismuth (III) nitrate pentahydrate (98%; Alfa Aesar Company, city, country), strontium carbonate (99%; Alfa Aesar Company), calcium nitrate tetrahydrate (Merck Company, city, country), strontium nitrate (Merck Company), magnesium nitrate hexahydrate (LACHEMA Company), ultra-pure water and bisphenol A (>= 99%, Sigma Aldrich). In addition to these, the others like nitric acid (65%), ethanol (absolute), acetonitrile (99.9%), and sodium hydroxide were bought from Merck Company.

2.2. Catalyst synthesis methods

Co-precipitation method was utilized to synthesis Bi_2O_3 catalyst. 1.94 g of $Bi(NO_3)_2.5H_2O$ weighed by precision balance. In addition, 1.12 M 20 mL HNO_3 (nitric acid-65%) solution and 0.2 M NaOH solution were prepared and kept in an ultrasonic bath for 15 min to ensure better dissolution. Finally, 20 mL of 1.12 molar HNO_3 solution was added to 1.94 of bismuth, which was weighed and then kept in the ultrasonic bath for 15 min. The solution of resulting were mixed by magnetic mixer at the room temperature. Subsequently, 0.2 M NaOH solution by adding drop by drop into the bismuth (III) nitrate solution was provided to reach pH value 11 and then mixed for 2 h at 75 °C to make a homogenous yellowish mixture. Then this mixture was filtered as well as washed with distilled water and absolute ethanol several times. Obtained this matter was dried in a oven at 80 °C for 2 h, then calcined at 450 °C for 2 h.

In order that preparing of binary catalyst, impregnation method was used. This method is based on impregnation of metal oxide solutions onto pure bismuth oxide catalyst. When preparing solutions, attention was paid to the weight percentages of metal oxides present in the binary catalyst. Firstly, nitrous forms of metal oxides ($Ca(NO_3)_2.4H_2O$, $Mg(NO_3)_2.6H_2O$, $Sr(NO_3)_2$) and 0.2 M solution of 5% by weight in binary catalyst were prepared. These solutions were added dropwise to the powdered pure bismuth oxide catalyst to give a wet mixture and then dried at 105 °C. This process was continued until the solutions were finished. It was then dried in oven at 105 °C for 16 h and then was calcined at 500 °C during 3 h.

2.3. Catalyst characterization

Total catalyst surface area of the catalysts was measured by nitrogen adsorption/desorption using a Quantachrome instrument. All catalysts were degassed under vacuum at 200 °C for 4 h.

Crystallographic structure of catalysts were determined by X-ray powder diffraction using CuKα radiation (λ = 1.54056 Å) with a Rigaku D/Max-2200 powder X-ray diffractometer. Before the analysis was run, the samples were gently granulated in an agate mortar to reduce the required orientation. Patterns were recorded at scan speed 2 degree of two-theta in the range of 10-90° 2θ. The average crystallite size (D_{avg}) was computed using the Debye–Scherrer equation.

The powders were examined with a high resolution scanning electron microscope (SEM) (JEOL/JSM-a6335F) for possible differences in morphologies and size distributions of the powders.

FT-IR spectra were examined by FT-IR spectroscopy (Perkin Elmer Precisely Spectrum One). KBr powder was used to prepare KBr pellets for samples. The samples were acquired as 100 scans with 4 cm^{-1} resolution

Optical energy gap of nano powders were carried out by a doublebeam UV-Shimadzu 3600 UV-vis-NIR spectrophotometer equipped a diffuse reflectance (DR) accessory.

The energy of band gap for the catalyst was evaluated by using the Kubelka–Munk formula with Tauc's relation (Eq. (1))

$$\left(hvF\left(R\alpha\right)\right)^{\frac{1}{n}} = A\left(hv - E_g\right)\left(hvF\left(R\alpha\right)\right)^{\frac{1}{n}} = A\left(hv - E_g\right) \quad (1)$$

In this expression, hν is the energy of a single proton, α is the optical absorption co-efficiency, E_g is the optical band gap energy, A is constant for direct band gap transitions, the value of exponent parameter n denotes the nature of sample transition (n = ½ is used for the catalyst). R is the absolute reflectance value; F(R) is proportional to the absorption coefficient (α).

Moreover, photoluminescence (PL) spectra were obtained on a Cary Eclipse fluorescence spectrophotometer (Agilent Technologies, city, country). The catalyst was excited by a xenon lamp light source by 450 nm at the room temperature.

2.4. Studies on photocatalytic activity

The experiment of BPA degradation was carried out over MxOy–Bi_2O_3 (M: Ca, Mg, Sr) binary oxide in a cylindrical quartz micro-photoreactor. Fifty mL of a 25 mg/L aqueous BPA solution was prepared and then 100 mg of catalyst was added in this mixture to initiate the reaction. Before exposure illumination, the solution was stirred in the dark for 1 h to establish an the adsorption-desorption equilibrium between the catalyst and the liquid. All reactions were conducted at ambient temperature under constant magnetic stirring and natural pH conditions. The photocatalytic activity of catalyst were compared using different light sources (UV-B, sunlight, and visible light irradiation). During the irradiation, sample was taken at regular intervals from the solution and filtered through a PTFE filter (pore size 0.45 mm for use total organic content (TOC) measurement (TOC-V, Shimadzu, city, country) and HPLC analysis. The analysis of BPA was performed by a HPLC (Thermo Scientific) using a C18 column. The mobile phase consists of a mixture of water and acetonitrile (40:60, v/v).

3. Results and discussion

3.1. Structural, morphological, and optical properties

The composition of the catalyst was determined using Thermo Elemental X Series ICP-MS. The actual weight percentages of the catalysts in the binary oxide catalysts were evaluated by ICP-MS analysis. The calculated wt% of the catalysts and the ICP-MS values were almost similar. Furthermore, ICP-MS values of the two representative catalysts clearly suggest that there may not be any noticeable differences between the calculated values and ICP values for the other weight percentages of metal oxides.

The diffraction patterns of powder samples were examined to identify the phase structures. XRD patterns representing this are show in Figure 1. Monoclinic α-Bi_2O_3 nanorods from corresponding to JCPDS files (No. 41-1449) was observed as the main crystalline phase. In addition, tetragonal MgO (JCPDS 45-0946), cubic CaO (JCPDS 82-1691), and tetragonal SrO (JCPDS 48-1477) were detected in the XRD analysis. The crystallite sizes of the catalysts are presented in Table.

After the impregnation of metal nitrate on Bi_2O_3, the lattice structure of Bi_2O_3 did not change. However, the average crystallite size of Bi_2O_3 changed with addition of metal oxide on Bi_2O_3. The crystallite size decreased with only the adding of metal oxide. After the XRD analysis, the crystallite sizes of samples were calculated as 41, 19, 17, and 15 nm for Bi_2O_3, 5MgO-Bi_2O_3, 5CaO-Bi_2O_3, 5SrO-Bi_2O_3, respectively. It has expressed that small crystallite size causes higher photocatalytic activity for the increased reactive sites and the promoted electron-hole separation efficiency [23].

Accordingly, the 5SrO-Bi_2O_3 binary oxide is expected to show higher photocatalytic activity due to its low crystallite size.

The morphology and particle size of Bi_2O_3, 5MgO-Bi_2O_3, 5CaO-Bi_2O_3, and 5SrO-Bi_2O_3 were observed by SEM in Figure 2a, Figure 2b, Figure 3c, and Figure 3d, respectively. Figure 2a exhibits the SEM photograph of samples. The morphology of pure Bi_2O_3 is purely a nanorod. The metal oxide particles were observed on the surface of nano Bi_2O_3.

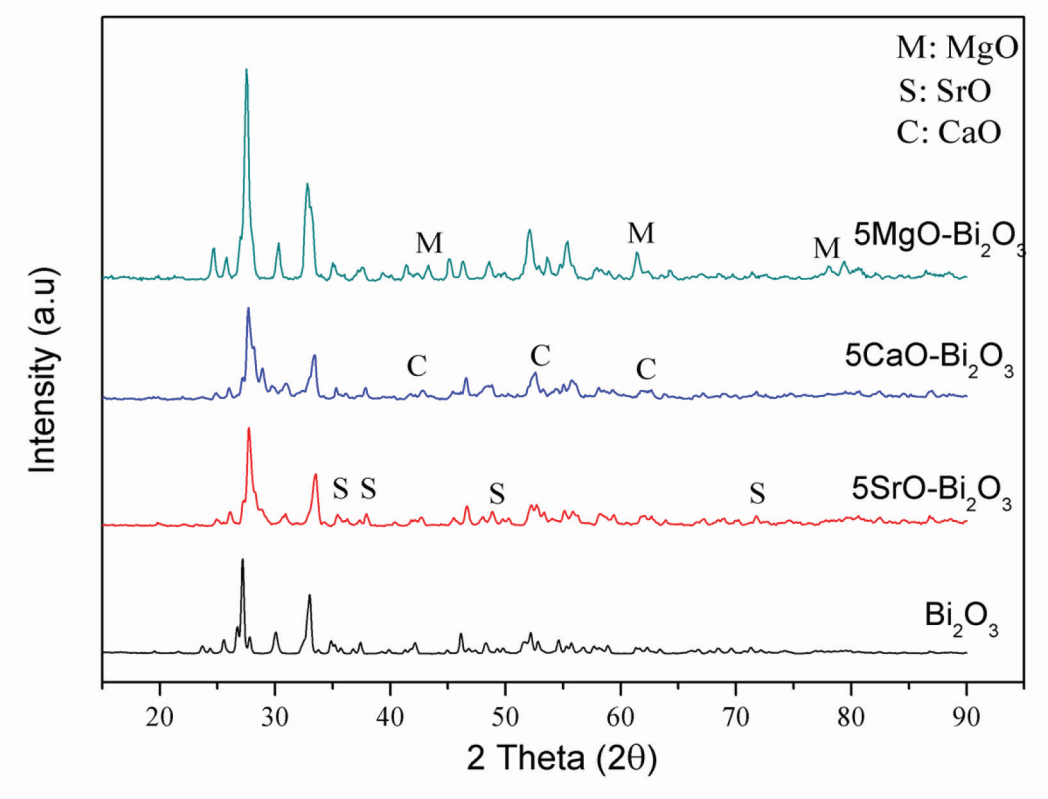

Figure 1. XRD patterns of Bi_2O_3, 5MgO-Bi_2O_3, 5CaO-Bi_2O_3, 5SrO-Bi_2O_3 catalysts.

Table. The crystallite size, specific surface area, band gap, morphology of materials, reaction rate constant, and Bisphenol-A (BPA) degradation efficiency over 30 min (%).

Catalyst	Crystallite size (nm)	S_{BET} (m^2g^{-1})	Band gap (eV)	BPA degradation efficiencies (%)	k_r ($mgL^{-1}min^{-1}$)
Bi_2O_3	41	15	2.99	76	0.037
5%MgO-Bi_2O_3	17	7	2.92	84	0.036
5%CaO-Bi_2O_3	19	10	2.88	88	0.069
5%SrO-Bi_2O_3	15	10	2.84	100	0.21

5SrO/Bi_2O_3 catalyst has uniform morphology whereas; 5CaO/Bi_2O_3 and 5Mg/Bi_2O_3 are in irregular sizes and shapes. It was observed that SrO was distributed over the surface of nano Bi_2O_3 compared to CaO and MgO. The homogeneous distribution of the SrO structure on the nano Bi_2O_3 surface has played a role in improving the high photocatalytic activity.

The change in the band gap energy of Bi_2O_3 with alkaline earth oxide loading was investigated using UV-vis diffuse reflectance spectroscopy. Figure 4 corresponds to UV-vis DRS spectra of the catalysts. The band gap energies of the samples were calculated from graphical extrapolation by using Tauc Plot ($(h\nu\alpha)^{1/n} = A(h\nu - E_g)$) adapted for Kubelka–Munk function [23]. The calculated band gap values are given in Table. According to the results, the band gap of pure Bi_2O_3 is 2.99 eV, whereas the band gap is decreased to 2.82 eV by the loading of 5 wt% SrO. The band gap of 5CaO/Bi_2O_3 and 5Mg/Bi_2O_3 are about 2.89, 2.92 eV, respectively. According these results, the loading of alkaline-metal oxide on Bi_2O_3 powder could significantly shift the optical band gap width E_g. It can be caused that the optical properties of the samples were affected by the quantum size, which is a consequence of the extent of the electron delocalization. As seen SEM image, MgO structure covered to Bi_2O_3 external surface. Therefore, the diffuse reflectance spectrum of 5MgO/Bi_2O_3 is more different than others. Because of the band gap value of Bi_2O_3, we studied the photocatalytic degradation of Bisphenol-A under UV irradiation.

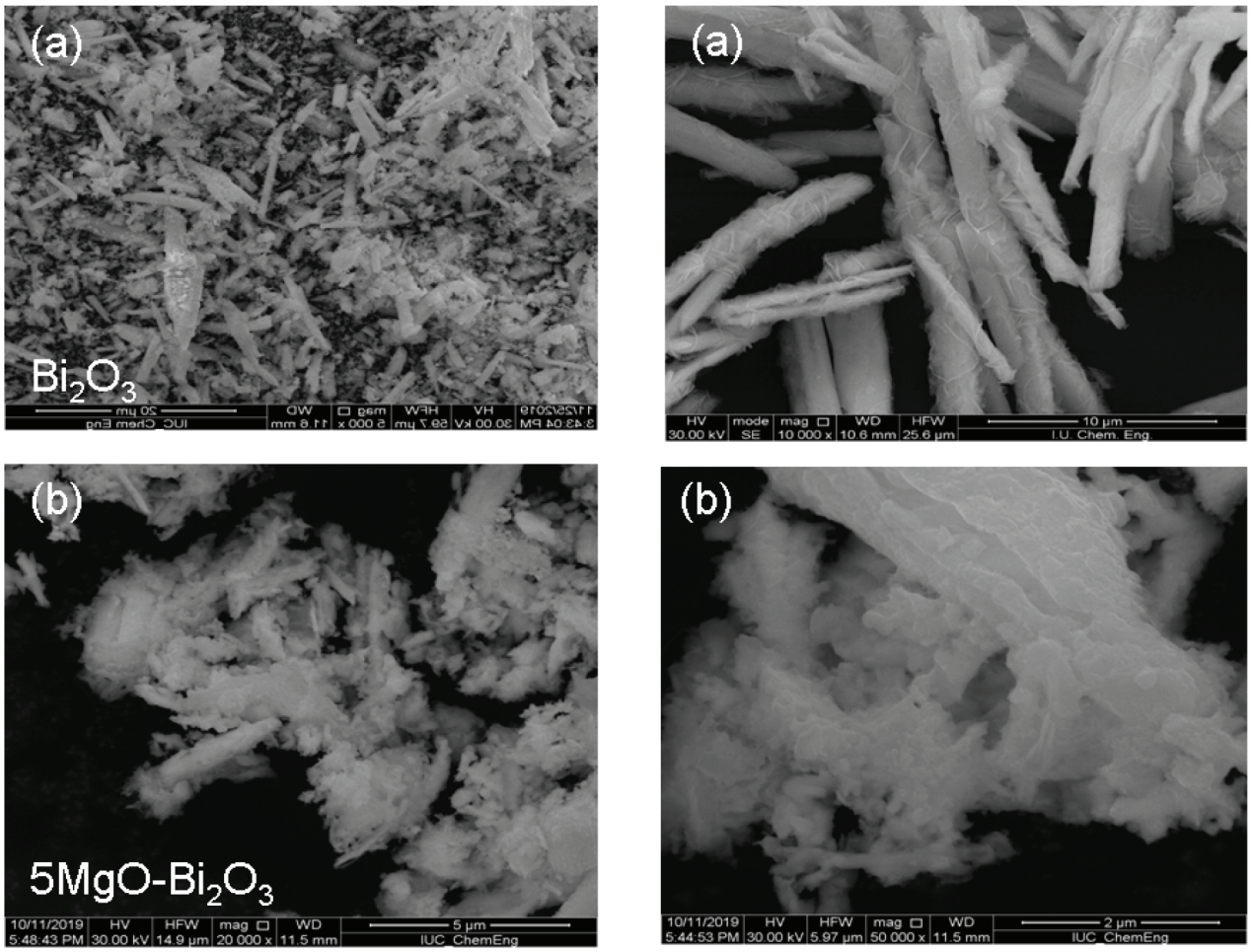

Figure 2. SEM images of (a) Bi_2O_3, (b) $5MgO\text{-}Bi_2O_3$ catalysts.

Figure 5 shows the FTIR spectra from 4000–400 cm^{-1} for pure Bi_2O_3 and alkaline earth oxide additive Bi_2O_3 catalysts. Infrared spectroscopy technology is used to detect the presence of functional groups such as hydroxyl radical (•OH) adsorbed on the surface of synthesized nanoparticles. In the photocatalytic degradation experiments, the surface OH groups can not only embrace the photogenerated holes to form hydroxyl radical (•OH) but also serve as active sites for the adsorption of reactants [24]. The intensive signal at around 1430–1445 cm^{-1} for all alkaline-doped catalyst was attributed to the absorption of non-bridging O-H groups [25]. The concentration of the hydroxyl group was affected by the addition of alkaline oxide to Bi_2O_3.OH bending appears in the spectra for $5SrO/TiO_2$ and $5CaO/Bi_2O_3$ catalyst at about 1439 cm^{-1}. However, this peak was not observed after MgO loading. These results are in line with the activity results.

In addition, the infrared spectrum of Bi_2O_3 was not observed any hydroxyl group. This result shows that the removing most of the adsorbed water from the surface of Bi_2O_3 with calcination process. In the spectrum, the band arises at 1300 cm^{-1} from the weak band of Bi–O–(NBO) bond in BO_3 units for $5CaO/Bi_2O_3$ and $5SrO/Bi_2O_3$. This peak was not observed for $5MgO/Bi_2O_3$. The low absorption band at around 830 cm^{-1} seemed in FTIR spectra of samples is the stretching vibration of Bi—O bonds in BiO_6 octahedral units [26]. The Bi—O bending vibration was observed at about 497, 537, and 830 cm^{-1} for Bi_2O_3. FTIR spectra of $5CaO/Bi_2O_3$ revealed the existence of peak at 874 cm^{-1} which are the characteristic bands of Ca-O [27]. In addition, the peak of the Sr-O band was observed at 857 cm^{-1} in the spectrum [28].

As a result of the FT-IR study, it was understood that Sr^{2+} and Ca^{2+}, except Mg^{2+}, entered into the lattice of nano Bi_2O_3.

The ionic radiuses of Sr^{2+} (1.21 Å) and Ca^{2+} (1.08) are larger than Bi^{3+} (1.03 Å) but less than O^{2-} (1.31 Å). These ions can homogenously substituted or introduced into the nano Bi_2O_3 matrix to produce oxygen vacancies that accelerate the transition and nanocrystalline growth of Bi_2O_3 [29].

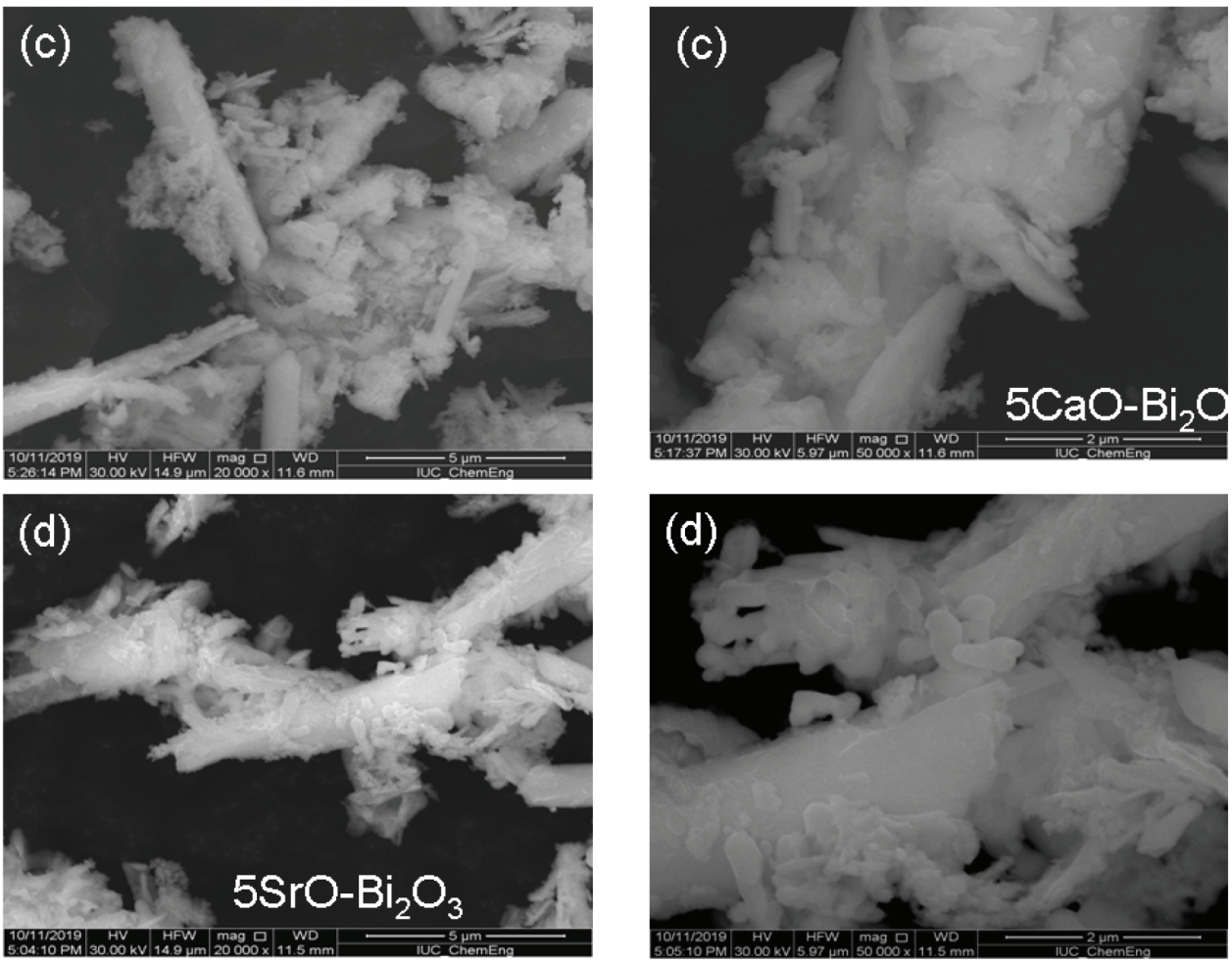

Figure 3. SEM images of (c) 5CaO-Bi_2O_3, (d) 5SrO-Bi_2O_3 catalysts.

The occurrence of Bi-O-Sr prevents the transition of Bi_2O_3 phase and prevents the agglomeration of nano Bi_2O_3 particles. There is no evidence for an isomorphic settlement of Mg^{2+} to the Bi_2O_3 structure observed due to the ionic radius of Mg^{2+}(0.86 Å) are lower than Bi^{3+} by adding Mg^{2+} to the nano Bi_2O_3 structure [30].

Photoluminescence spectroscopy is a widely used technique for characterization of optical and electronic properties of semiconductors and molecules. Photoluminescence can measure the purity and crystal quality of semiconductors and give some information oxygen vacancies, photo-induced charge carrier separation, and recombination processes surface states in nano-sized semiconductor materials. At low Pl density, the recombination rate of the electron hole is also low [31].

PL spectra of the catalysts are shown in Figure 6. It was understood that the PL emission spectra of the catalysts were at the same peak maximum but different densities. A strong emission peak at about 393 nm was obtained in the PL spectrum of the catalysts. It was determined that the density of the 5SrO-Bi_2O_3 catalyst in the emission spectrum was the lowest and this decrease showed the low recombination rate of the holes. As a result, it can be said that the 5SrO-Bi_2O_3 catalyst helps inhibit the recombination of electrons and holes and improve photocatalytic activity.

3.2. Photocatalytic activity results

The photocatalytic activity of alkaline earth oxides loaded Bi_2O_3 was examined for Bisphenol A degradation. We based on Langmuir–Hinshelwood (L-H) kinetic model [32] in our experiments. It can be expressed by Equation 2 below:

$$\ln(C_o/C) = k_{obs}t \quad (2)$$

Assuming that $C = C_o$ at $t = 0$ with low initial BPA concentration, where t is the given irradiation time and k_{obs} is the rate constant of the observed pseudo-first order reaction. After experiments, we calculated the photocatalytic degradation

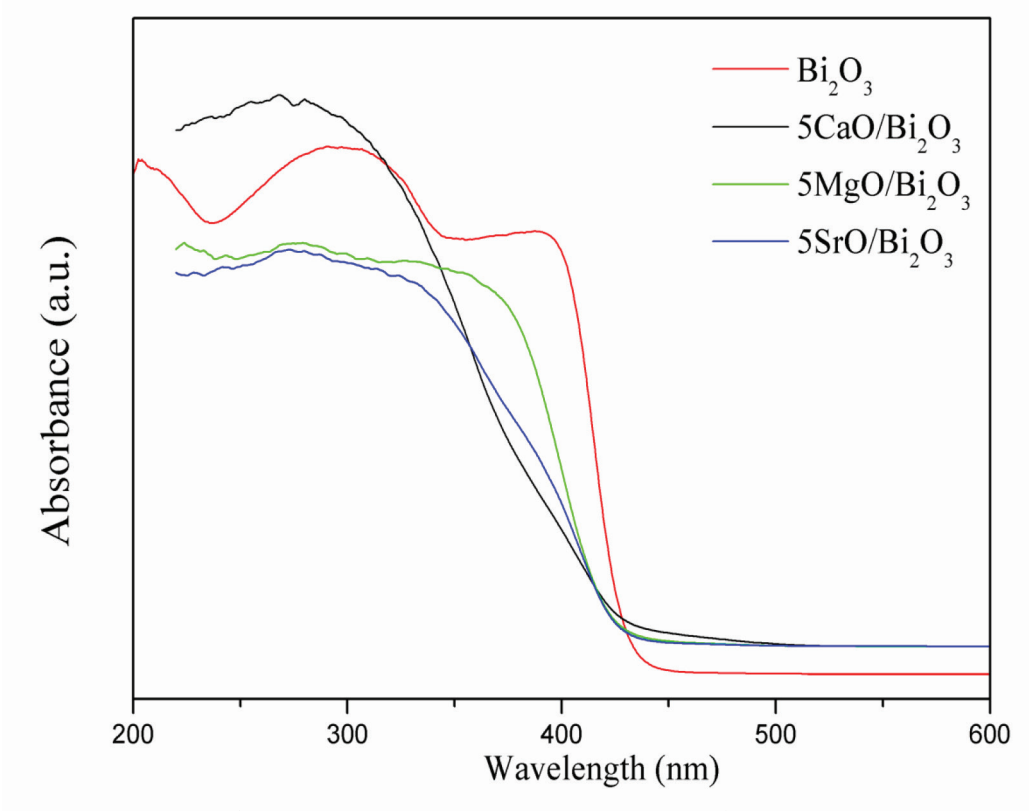

Figure 4. DRS spectra of Bi_2O_3, 5MgO-Bi_2O_3, 5CaO-Bi_2O_3, 5SrO-Bi_2O_3 catalysts.

efficiencies and reaction rates for the different photocatalysts and the numerical values of gain are presented in Table.

The degradation efficiency (R%) of BPA was calculated by Equation (3):

$$R\% = \frac{C_o - C}{C_o} \quad (3)$$

Firstly, we tested UV-B light and visible light as the different light source for degradation of BPA by using pure Bi_2O_3 and the degradation efficiencies of pure Bi_2O_3 were 76% and 47% for 30 min, respectively. The activity results show that although Bi_2O_3 can be activated under different irradiation, it is not sufficient for complete of BPA.

Moreover, we studied with SrO-Bi_2O_3 binary oxide prepared with varying SrO loadings. The degradation efficiency for the SrO-Bi_2O_3 binary oxide increased with the rise in the amount of SrO charges to Bi_2O_3. It showed the highest percentage of BPA degradation (100%) in 30 min with a loading of 5% by weight SrO. However, there was no significant change in activity after this weight percentage and the value remained the same as the higher loading of SrO. The numerical values of gain showed that the structural and optical characterization of the samples and SrO dispersion on the surface affected with the loading of SrO in the binary oxide.

In addition, the performance of 5SrO-Bi_2O_3 catalyst was studied with UV-B light and visible light for BPA degradation. According the experimental results, binary metal oxide nanoparticles are more photoactivated under UV light than visible light irradiation. The degradation of BPA under visible light and UV-B light (64 W) showed 35% and 100% for 30 min, respectively.

In addition, the reusability of the 5SrO-Bi_2O_3 catalyst was studied on fresh dye samples (5 trials). 5SrO-Bi_2O_3, when used for the first time, could degrade 98.52% BPA, with a small change (to 94.29%) in the efficiency when used for 5 times. This decrease in the efficiency for 5SrO-Bi_2O_3 catalyst resulted probably from the photocorrosion effect.

In this study, the photodegradation of BPA includes three steps. In the first stage, the transmission of electrons excited by photons emitted from the UV-B source from the valence band to the conduction band takes place. In the second stage, the holes formed due to the excitation process act as decomposing agent or combine with the surface hydroxyl species on the binary oxide to form the hydroxyl radical. In the last stage, the contaminant is attracted by the holes or hydroxyl radicals by the photons from the UV-B source.

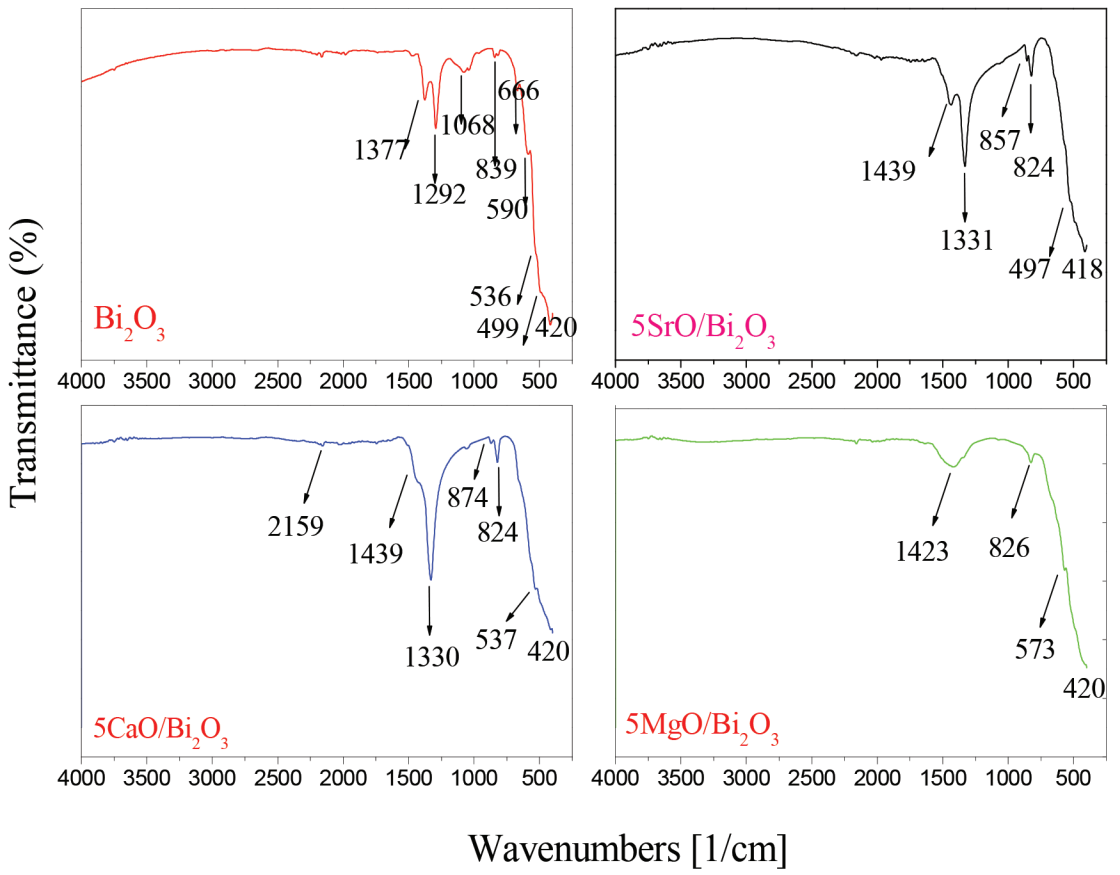

Figure 5. FTIR spectra of Bi_2O_3, 5MgO-Bi_2O_3, 5CaO-Bi_2O_3, 5SrO-Bi_2O_3 catalysts.

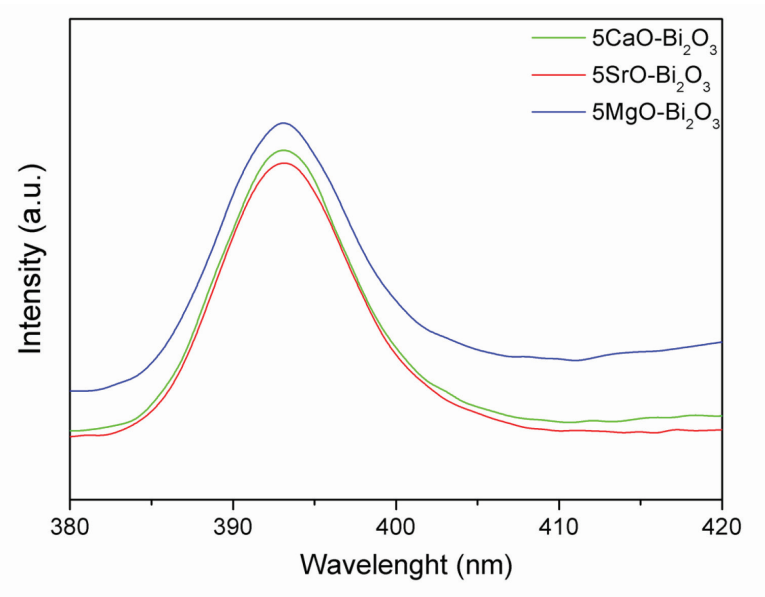

Figure 6. Photoluminescence spectrum of Bi_2O_3, 5MgO-Bi_2O_3, 5CaO-Bi_2O_3, 5SrO-Bi_2O_3 catalysts.

Figure 7a shows the photocatalytic degradation of BPA in the pure Bi_2O_3 and alkaline earth oxide additive Bi_2O_3 catalysts under UV-B illumination at different irradiation times. When the degradation results are evaluated, the photocatalytic degradation rates of the BPA in 30 min with the binary metal oxides are sorted in descending order: 5SrO—Bi_2O_3 (ca. 100%), 5CaO—Bi_2O_3 (ca. 88%), 5MgO—Bi_2O_3 (ca. 84%), and Bi_2O_3 (ca. 76%). Obviously, 5SrO—Bi_2O_3 catalyst improved the degradation of BPA in a short time and with high efficiency compared to other catalysts and pure Bi_2O_3. The results show that •OH radical adsorbed on the catalyst was play an extreme role in the photodegradation of BPA. A small difference in the efficiency during the photocatalytic degradation of BPA can be elucidated by the free •OH radicals involved to a small extent in the photodegradation process [33].

The measured TOC removal results for the photodegradation of BPA with 5SrO—Bi_2O_3, 5CaO—Bi_2O_3, and 5MgO—Bi_2O_3 are shown in the Figure 7b. Twenty-five ppm BPA completely decomposed in 30 min with 5SrO—Bi_2O_3 binary oxide and 94% TOC removal was obtained in 30 min. It is clear that the total mineralization is completed in the presence of 5SrO—Bi_2O_3 catalyst.

The acid-base properties of the oxide catalyst can also affect the photocatalytic activity as well as its structural and optical properties.

As known, alkalinity of alkaline earth oxide increases from MgO to SrO. It seems that the activity changes in parallel with the alkalinity. As a result, the addition of strong basic alkaline oxide caused an increase in both the photocatalytic activity and the final conversion in oxidative degradation of BPA over catalysts. In addition to this result, the tendency of MgO to form larger particles on Bi_2O_3 surface also caused a decrease in BPA conversion.

In the study, it was understood that the changes in surface area, band gap energy, and crystallite size were not as much as the changes in catalytic activity. These differences in activity are thought to be due to the active species on the surface of the oxide mixtures.

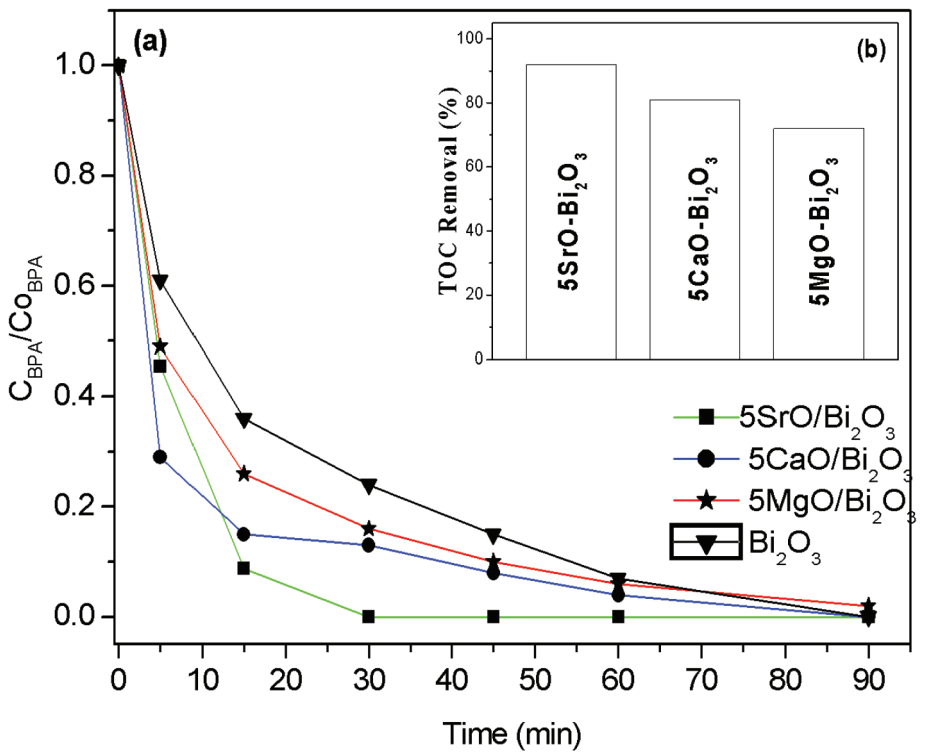

Figure 7. (a) Degradation activities of Bi_2O_3, 5MgO-Bi_2O_3, 5CaO-Bi_2O_3, 5SrO-Bi_2O_3 catalysts. (b) Inset shows the impact of surfactant on TOC removal in the BPA degradation.

4. Conclusions

The effects of different alkaline-earth oxide doped with Bi_2O_3 nanoparticles on the photocatalytic degradation of bisphenol A were investigated. SrO-Bi_2O_3, CaO-Bi_2O_3, and MgO-Bi_2O_3 binary oxides were prepared by wet-impregnation method. The photocatalytic activities of the catalysts were compared for different light sources. Considering that the characterization analysis and improved photocatalytic activity results are mainly varied in relation to the effective structure of SrO-Bi_2O_3 binary oxide and the strong basic properties in the nanocomposite. Obviously, 5wt% SrO-Bi_2O_3 photocatalyst showed more excellent degradation performance and highest degradation reaction rate (0.21 mg l^{-1} min^{-1}) within 30 min. It was observed that the photocatalytic activity improved by the addition of alkaline-earth oxide on Bi_2O_3.

In this study, Sr^{2+} played an important role in reducing the crystallite size of nano Bi_2O_3. The small particle size of 5SrO-Bi_2O_3 and uniformly distribution of SrO on the pure nano Bi_2O_3 surface were very effective in the short time and complete degradation of BPA. The findings of this study elucidated an approach for the removal of BPA in the water through photocatalytic of degradation by alkaline-earth oxide doped with Bi_2O_3.

Acknowledgment

This work was supported by the Scientific Research Projects Coordination Unit of Istanbul University-Cerrahpaşa.

References

1. Vanderberg LN, Hauser R, Marcus M, Olea N, Welshons WV. Human exposure to bisphenol A (BPA). Reproductive Toxicology 2017; 24: 139-177. doi: 10.1016/j.reprotox.2007.07.010
2. Zielińska M, Wojnowska-Baryła I, Cydzik-Kwiatkowska A. Bisphenol A removal from water and wastewater. Springer International Publishing, Switzerland 2019. doi: 10.1007/978-3-319-92361-1
3. Wilson C. BPA-free water bottles may be harmful too. Nature Communications 2017; 3115. doi: 10.1038/ncomms14585
4. Ortiz-Martínez K, Reddy P, Cabrera-Lafaurie WA, Román FR, Hernández-Maldonado AJ. Single and multi-component adsorptive removal of bisphenol A and 2,4-dichlorophenol from aqueous solutions with transition metal modified inorganic–organic pillared clay composites: effect of pH and presence of humic acid. Journal of Hazardous Materials 2016; 312: 262-271. doi: 10.1016/j.jhazmat.2016.03.073
5. Venkat Savunthari K, Shanmugam S. Effect of co-doping of bismuth, copper and cerium in zinc ferrite on the photocatalytic degradation of bisphenol A. Journal of the Taiwan Institute of Chemical Engineers 2019; 101: 105-118. doi: 10.1016/j.jtice.2019.04.042
6. Cotman M, Erjavec B, Djinovic P, Pintar A. Catalyst support materials for prominent mineralization of bisphenol A in catalytic ozonation process. Environmental Science and Pollution Research 2016; 23: 10223-10233. doi: 10.1007/s11356-016-6251-y
7. Darsinou B, Frontistis Z, Antonopoulou M, Konstantinou I, Mantzavinos D. Sono-activated persulfate oxidation of bisphenol A: kinetics, pathways and the controversial role of temperature. Chemical Engineering Journal 2015; 280: 623-633. doi: 10.1016/j.cej.2015.06.061
8. Shuo L, Zhang G, Wang P, Zheng H, Zheng Y. Microwave-enhanced Mn-Fenton process for the removal of BPA in water. Chemical Engineering Journal 2016; 294: 371-379. doi: 10.1016/j.cej.2016.03.006
9. Liu Y, Zhong G, Liu Z, Meng M, Liu F et al. Facile synthesis of novel photoresponsive mesoporous molecularly imprinted polymers for photo-regulated selective separation of bisphenol A. Chemical Engineering Journal 2016; 296: 437-446. doi: 10.1016/j.cej.2016.03.085.
10. Dai Y, Yao J, Song YH, Liu X, Wang S et al. Enhanced performance of immobilized laccase in electrospun fibrous membranes by carbon nanotubes modification and its application for bisphenol A removal from water. Journal of Hazardous Materials 2016; 317: 485-493. doi: 10.1016/j.jhazmat.2016.06.017
11. Wang X, Tang P, Ding C, Cao X, Yuan S et al. Simultaneous enhancement of adsorption and peroxymonosulfate activation of Nitrogen-doped reduced graphene oxide for bisphenol A removal. Journal of Environmental Chemical Engineering 2017; 5: 4291-4297. doi: 10.1016/j.jece.2017.08.018
12. Suganya Josephine GA, Jayaprakash K, Suresh M, Sivasamy A. Photocatalytic degradation of 2,4-dicholorophenoxyacetic acid: a herbicide by nanocrystalline semiconductor material under visible light irradiation. Materials Today: Proceedings 2019; 17: 345-353. doi: 10.1016/j.matpr.2019.06.440
13. Shtarev DS, Shtareva AV, Syuy AV, Pereginiak MV. Synthesis and photocatalytic properties of alkaline earth metals bismuthates–bismuth oxide compositions. Optik 2016; 217. 1414-1420. doi: 10.1016/j.ijleo.2015.10.075
14. Liu J, Xie F, Li R, Li T, Jia Z et al. TiO_2-x/Ag_3PO_4 photocatalyst: oxygen vacancy dependent visible light photocatalytic performance and BPA degradative pathway. Materials Science in Semiconductor Processing 2019; 97: 1-10. doi: 10.1016/j.mssp.2019.03.002
15. Nguyen TB, Huang CP, Doong R. Photocatalytic degradation of bisphenol A over a $ZnFe_2O_4$/TiO_2 nanocomposite under visible light. Science of The Total Environment 2019; 646: 745-756. doi: 10.1016/j.scitotenv.2018.07.352

16. Lee JM, Kim MS, Kim BW. Photodegradation of bisphenol-A with TiO_2 immobilized on the glass tubes including the UV light lamps. Water Research 2004; 38: 3605-3613. doi: 10.1016/j.watres.2004.05.015

17. Coronado-Castañeda RRS, Maya-Treviño ML, Garza-González E, Peral J, Villanueva-Rodríguez M, Hernández-Ramírez A. Photocatalytic degradation and toxicity reduction of isoniazid using β-Bi_2O_3 in real wastewater. Catalysis Today 2020; 341: 82-89. doi: 10.1016/j.cattod.2019.01.028

18. Owolabi TO, Gondal MA. A hybrid intelligent scheme for estimating band gap of doped titanium dioxide semiconductor using crystal lattice distortion. Computational Materials Science 2017; 137: 249-256. doi: 10.1016/j.commatsci.2017.05.047

19. Xiao X, Hu R, Tu S, Zheng C, Zhong H et al. One-pot synthesis of micro/nano structured β-Bi_2O_3 with tunable morphology for highly efficient photocatalytic degradation of methylparaben under visible-light irradiation. RSC Advances 2015; 5: 48. doi: 10.1039/C5RA03200H

20. Xiao X, Hu R, Liu C, Xing C, Qian C et al. Facile large-scale synthesis of β-Bi_2O_3 nanospheres as a highly efficient photocatalyst for the degradation of acetaminophen under visible light irradiation. Applied Catalysis B: Environmental 2013; 140-141: 433-443. doi: 10.1016/j.apcatb.2013.04.037

21. Jalalah M, Faisal M, Bouzid H, Park JG, Al-Sayari SA et al. Comparative study on photocatalytic performances of crystalline α- and β-Bi_2O_3 nanoparticles under visible light. Journal of Industrial and Engineering Chemistry 2015; 30: 183-189. doi: 10.1016/j.jiec.2015.05.020.

22. Yu J, Xiong J, Cheng B, Liu S. Fabrication and characterization of Ag-TiO_2 multiphase nanocomposite thin films with enhanced photocatalytic activity. Applied Catalysis B-Environmental 2005; 60: 211-221. doi: 10.1016/j.apcatb.2005.03.009

23. López R, Gomez R. Band-gap energy estimation from diffuse reflectance measurements on sol–gel and commercial TiO_2: a comparative study. Journal of Sol-Gel Science and Technology 2011; 61: 1-7. doi: 10.1007/s10971-011-2582-9

24. Cao L, Spiess FJ, Huang A, Suib SL, Obee TN et al. Heterogeneous photocatalytic oxidation of 1-Butene on SnO_2 and TiO_2 films. The Journal of Physical Chemistry B 1999; 103 (15): 2912-2917. doi: 10.1021/jp983860z

25. Ivanova T, Harizanova A, Koutzarova T, Vertruyen B. Effect of annealing temperatures on properties of sol-gel grown ZnO-ZrO_2 films. Crystal Research and Technology 2010; 45: 1154-1160. doi: 10.1002/crat.201000427

26. Zhang L, Wang W, Yang J, Chen Z, Zhang W et al. Sonochemical synthesis of nanocrystallite Bi_2O_3 as a visible-light-driven photocatalyst. Applied Catalysis A: General 2006; 308: 105-110. doi: 10.1016/j.apcata.2006.04.016

27. Nyquist RA, Kagel RO, 1997. The Handbook of Infrared and Raman Spectra of Inorganic Compounds and Organic Salts, Academic Press Inc., New York.

28. Rahman MM, Hussain MM, Asiri AM. A novel approach towards hydrazine sensor development using SrO·CNT nanocomposites. Royal Society of Chemistry 2016; 70: 65291-65298. doi: 10.1039/C6RA11582A

29. Francisco MSP, Mastelaro VR. Inhibition of the anatase–rutile phase transformation with addition of CeO_2 to CuO–TiO_2 system: Raman spectroscopy, X-ray diffraction, and textural studies. Chemistry of Materials 2002; 14: 2514-2518.

30. Pauling L. 1960. The nature of the chemical bond and the structure of molecules and crystals, third ed. Cornell University Press, New York.

31. Fujihara K, Izumi S, Ohno T. Matsumura M. Time-resolved photoluminescence of particulate TiO_2 photocatalysts suspended in aqueous solutions. Journal of Photochemistry and Photobiology A: Chemistry 2000; 132: 99-104. doi: 10.1016/S1010-6030(00)00204-5

32. Patil MR, Khairnar SD, Shrivastava VS. Synthesis, characterisation of polyaniline-Fe_3O_4 magnetic nanocomposite and its application for removal of an acid violet 19 dye. Applied Nanoscience 2015; 6 (4): 495-502. doi: 10.1007/s13204-015-1465-z

33. Chen Y, Yang S, Wang K, Lou L. Role of primary active species and TiO_2 surface characteristic in UV-illuminated photodegradation of acid orange 7. Journal of Photochemistry and Photobiology A: Chemistry 2005; 172: 47-54. doi: 10.1016/j.jphotochem.2004.11.006